A micromechanics-based model for creep behavior of rock

H Yoshida and H Horii
Department of Civil Engineering, University of Tokyo
7-3-1 Hongo, Bunkyoku, Tokyo, Japan

Recently, various ideas on underground development have been proposed and associated technical problems have been studied. One of the issues of concern is the prediction of the long-term behavior of rock, such as creep phenomena and fatigue. The mechanical behavior of rock is known to be greatly affected by temperature, confining pressure, pore fluid pressure and pH. It is necessary to establish a prediction method for creep deformation and creep failure of rock in order to ensure the long-term safety of the underground structures such as vaults for nuclear waste and power stations.

Studies with the scanning electron microscope (SEM) revealed that the mechanisms of creep deformation and creep failure is the growth of microcrack nucleated at a pre-existing defect. Under compression below the failure strength, the microcrack gradually grows and the rock specimen fails after a certain time. The mechanism of time-dependent crack growth is understood as the stress corrosion at the crack tips.

The objective of this study is to establish a prediction method of creep behavior. It is necessary to understand the governing mechanism of phenomena and to build a model for the reproduction of creep behavior. In the present study, an analytical model of microcrack growth under compression on the basis of micromechanics is proposed. The analytical results of the proposed model are compared with the experimental results. It appears that the experimental data are reproduced by the model.

Moreover, a constitutive equation is derived from the proposed micromechanical model and is implemented into a finite element program to analyze the creep behavior of underground structures. As an example, a problem of elliptical excavation under hydrothermal conditions is analyzed and a crack length field is predicted as a function of time at different temperatures. It is concluded that the results of the finite element analysis indicate the possibility that rock may fail due to the effect of high temperature.

1 INTRODUCTION

Recently, various ideas on underground use and development have been proposed and associated technical problems have been studied; for example, the storage of low temperature gas, the construction of research center related to nuclear power projects, the storage of electricity using the superconductivity, the Hot Dry Rock (HDR) geothermal extraction and the disposal of nuclear waste in vaults in hard rock.

For underground structures which require long-term stability, such as the disposal of nuclear waste, it is important to inquire the time-dependent behavior of rock, such as creep phenomena and fatigue.

Furthermore, the knowledge of the mechanical properties of rock under hydrothermal conditions is required to develop design methodology for nuclear waste repository and HDR geothermal reservoir. One of the issues of concern is the prediction of the long-term behavior or the behavior under hydrothermal conditions of rock. From the engineering point of view, it is required to focus on the creep phenomena which is time-dependent behavior and considered to be greatly affected by the temperature. In order to predict such phenomena, it is necessary to comprehend the mechanism which governs such phenomena and build analytical model to reproduce it.

Rock is known to be heterogeneous containing grain boundaries, pores, flaws, cavities, inclusions, and microcracks. The mechanical behavior of rock, such as macroscopic failure and dilatancy, are known to be greatly affected by temperature, confining pressure, pore fluid pressure, and pH. Rock fails under axial compression by axial splitting when the confining pressure is zero or very small and by faulting or shear failure when the confining pressure is moderate but below the brittle-ductile transition value. Larger

"Micromechanical modelling of quasi-brittle materials behavior" edited by Victor C Li, ASME Book No AMR118 $60 (members $30)
Appl Mech Rev vol 45, no 8, August 1992

confining pressure causes plastic deformation and brittle-ductile failure occur.

Recent experimental researches with optical and electron microscopes and acoustic emission, have produced a large mount of information on mechanical properties of rock. Electron Scanning Microscopy (SEM), above all, enables us to observe the sources of initial defects and their growth in response to applied loads (see, for example, Tapponnier and Brace [1976], Krantz [1979]). Tapponnier and Brace investigated the development of stress-induced microcracks in Westerly granite with the SEM [1976]. They reported that sets of grain boundary, low-aspect ratio cavities, as well as suitably oriented interfaces of two different minerals, produce most microcraks. When rock is subjected to compressive stresses, extensile, opening mode cracks grow from pre-existing defects and overall stiffness is reduced. Moreover, studies with SEM revealed that the mechanisms of creep deformation and creep failure are also attributed to microcracking nucleated at a pre-existing defect. Krantz [1979, 1980] carried out a creep test for Barre granite at room temperature with and without confining pressure and made a detailed microscopic observation of crack growth. It was shown that creep behavior in brittle rock is caused by crack growth due to corrosive reactions at the crack tips.

Various mathematical models based on microscopic observations have been introduced to analyze the failure phenomena under compression, such as shear failure, axial splitting, and brittle-ductile transitions of materials. Most of them are based on the idea that the frictional sliding of the pre-existing defects causes the crack growth in the direction of the maximum compression. Nemat-Nasser and Horii [1982a] and Horii and Nemat-Nasser [1985,1986] have studied extensively the growth of crack emanating from a flaw with frictional and cohesive resistance. The model is formulated as a two-dimensional elasticity problem and the numerical results are compared with those of model experiments. They reported that, under axial compression, tension cracks nucleate at the tips of the pre-existing flaws which have frictional resistance and grow in the direction of maximum principal stress. When lateral compression is present, the crack growth is stable and stops at a certain crack length which is reduced at higher confining pressure. With a small lateral tension, on the other hand, the crack growth becomes unstable after some finite crack length is attained. To model faulting observed in the presence of a confining pressure, they considered the interaction effect of a row of flaws and calculated the length of the tension cracks which were nucleated at the crack tips and growing with increasing axial load.

The understanding and description of the failure mechanism of rock have long been a goal in the field of rock mechanics. The main purpose of this study is to establish a prediction method for creep behavior of hard rock based on the micromechanics of creep deformation and creep failure. The analytical model of rock under compression to reproduce creep behavior is proposed. It is noted that microstructural parameters such as crack density and size of a pre-existing defect play an important role in rock behavior. In this paper, on the basis of the experimental results by Krantz [1979, 1980], the input parameters are determined. The numerical results of the proposed model are compared favorably with the experimental results by Krantz. Furthermore, with the proposed model, a constitutive equation of creep deformation and a criterion of creep failure are constructed and implemented into a finite element program to analyze the creep behavior of underground structures under hydrothermal environment. As an example, a problem of elliptical excavation under hydrothermal conditions is analyzed by the finite element program and the crack length field is predicted as a function of time at different temperatures.

2 MECHANISM OF CREEP BEHAVIOR

2.1 Crack growth

Most rock exhibits time-dependent fracture. That is, when a rock specimen is subjected to a static load, it fails after a time interval that depends on the magnitude of the load. Krantz [1979] conducted uniaxial creep tests on granite in the following manner. A number of cylindrical samples of Barre granite were cored from the same block in the same direction, and both axial and radial strains, parallel and perpendicular to the long axis of the cylinders, were measured. Each sample was loaded to a constant stress which was equivalent to approximately 87% of the uniaxial fracture strength at room temperature and pressure. Samples were unloaded at different moments during the test, and the surface inside the specimen was cut out and observed with the SEM.

Figure 1 shows the relationship between the radial strain and time. The radial strain increases with increasing time and finally the specimen fails at a certain time. The failure time depends on the applied stress so that a smaller applied axial compression results in a longer failure time.

Krantz reports that the orientation of the cracks is more or less random before loading. After the application of load, it is almost parallel to the axial compression. This means that, under axial compression, tension cracks emanate from the tips of pre-existing defects (grain boundaries, pores, flaws, cavities, inclusions, microcracks, etc), and propagate in a direction parallel to the maximum compression. With increasing time, the average length of cracks increases. Distribution of microcracks is more or less

uniform up to the final stage. The final failure is accompanied by change from uniform cracking to localized cracking. The SEM observation by Krantz revealed that the creep deformation and creep failure of hard rock are due to microcracking.

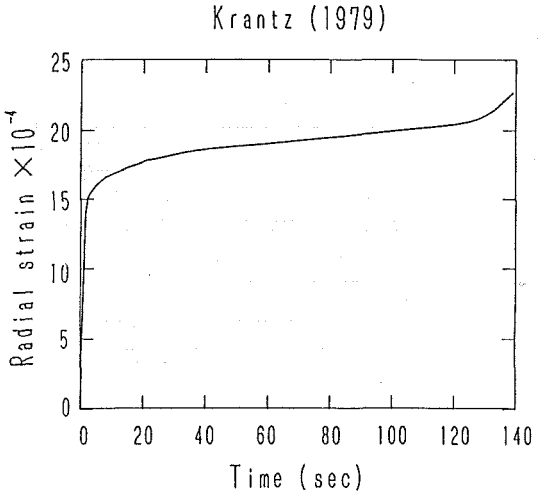

Figure 1 Radial strain as a function of time in creep test

Krantz also performed creep tests with various confining pressures and axial stresses to study the effect of confining pressure and stress difference on the creep behavior of granite. It is reported that the effect of pressure is to increase creep failure time and increase the amount of inelastic deformation of rock before instability. This increased deformation is due to longer and more numerous microcracks. The tendency is the same with different confining pressures. The failure time depends not only on loading conditions but also on temperature and environmental conditions such as humidity and pH.

2.2 Stress corrosion cracking

A crack grows at a certain slow speed when the stress intensity factor is less than the fracture toughness. This phenomenon is referred to as time-dependent crack growth, subcritical crack growth, stable cracking, or quasi-static crack propagation.

Studies with electron microscope revealed that the time-dependent crack growth in rock is the stress corrosion crack growth. Stress corrosion provides a mechanism by which cracks can grow under loads that are too small to break bonds at the crack tip. By introducing a chemically corrosive agent, such as water, to the crack tip, the bond energy is reduced and bonds can be broken at a reduced stress level. The velocity of crack growth is controlled by the rate of the stress corrosion at the crack tips. The crack velocity is a function of the stress intensity factor when the stress intensity factor is below the fracture toughness. If they are plotted in log-log diagram, it is best reproduced by a straight line shown in Figure 2.

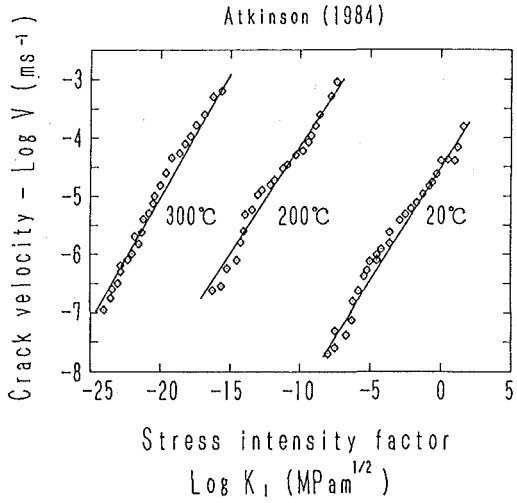

Figure 2 Crack velocity as a function of time

Therefore, the stress corrosion crack growth is described by the following power law.

$$\frac{dl}{dt} = A(K_I)^n \tag{2.1}$$

where dl/dt is the velocity of the crack, K_I is the stress intensity factor of Mode I, A and n, stress corrosion indices, are considered to be the material constants. The stress intensity factor depends on the geometry and magnitudes of stresses. It is known that the velocity of crack growth changes with temperature and environmental conditions such as humidity and pH. Hence A and n are considered to be a function of those parameters. In this study, an analytical model of time-dependent crack growth under compression is proposed based on the mechanism of stress corrosion crack growth.

3 MODEL OF CREEP

3.1 Micromechanical model of crack growth under compression

Various kinds of inhomogeneities that exist in rock - such as grain boundaries, the different types of grains, pores, flaws, cavities, and inclusions with different orientations - play roles in the mechanical behavior of rock samples. Under axial compression, the frictional sliding and the plastic deformation that occur at those microstructures produce the tensile stress locally and this causes microcracks to nucleate and grow in the direction of maximum compression.

Figure 3 shows the mechanism of propagation of a stress-induced microcrack at a biotite grain boundary in quartz.

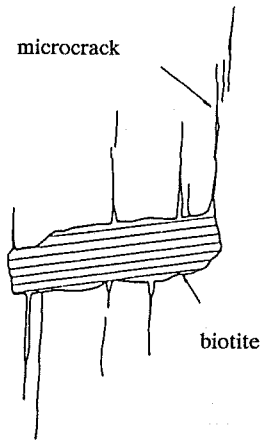

Figure 3 Stress-induced microcrack at a biotite grain boundary (from Tapponnier and Brace)

On the basis of the microscopic observations, Horii and Nemat-Nasser (1986) proposed a simple two-dimensional model to analyze crack growth resulted from the slip along a pre-existing defect and explained splitting in terms of unstable crack growth due to existing local tension. They also showed that crack growth becomes unstable due to the interaction between microcracks even under triaxial compression. It leads to the formation of a localized cracking region, which governs the strength of a material and becomes the final failure plane.

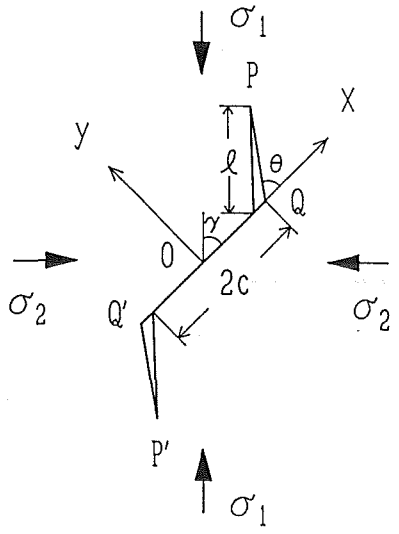

Figure 4 Crack growth model under compression

Figure 4 shows the micromechanical model of crack growth proposed by Horii and Nemat-Nasser[1986]. Under maximum and minimum principal compression σ_1 and σ_2 which are negative, PP' is a pre-existing defect of length 2*c*, and both PQ and P'Q' are tension cracks of length *l*. The boundary conditions on the pre-existing defect PP' are

$$u_y^+ = u_y^- \qquad \tau_{xy}^+ = \tau_{xy}^- = -\tau_c + \mu\sigma_y \tag{3.1}$$

and the boundary condition on cracks PQ and P'Q' is

$$\sigma_\theta = \tau_{r\theta} = 0 \tag{3.2}$$

where u_y is the displacement in the *y*-direction, τ_c is the cohesive stress, μ is the coefficient of friction, σ_y and τ_{xy} are the normal and shear stresses on PP', and σ_θ and $\tau_{r\theta}$ are the polar components of the normal and shear stresses on PQ and P'Q'. The superscript plus and minus indicate the value of the quantity on the upper and lower faces, respectively.

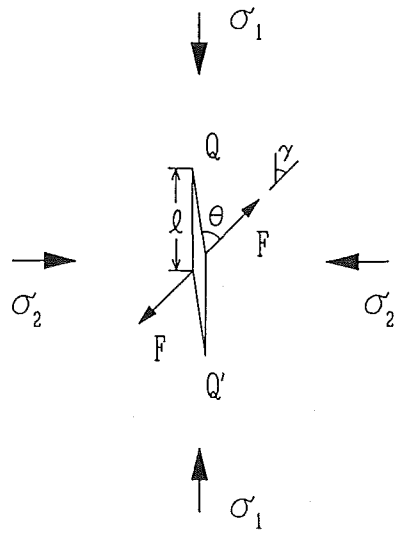

Figure 5 Simplified crack growth model under compression

Furthermore, Horii and Nemat-Nasser also considered a simpler model with a single crack QQ' of length 2*l*, subjected at its center to a pair of the collinear splitting force, *F*, which makes an angle γ with the σ_1-direction (see, Figure 5). These forces represent the effect of the sliding of the pre-existing defects PP'. *F* is calculated by estimating the driving shear stress τ^* along the pre-existing defect due to the friction, as follows:

$$F = 2c\tau^*,$$

$$\tau^* = -\frac{1}{2}(\sigma_1-\sigma_2)\sin 2\gamma - \tau_c + \frac{\mu}{2}[\sigma_1+\sigma_2-(\sigma_1-\sigma_2)\cos 2\gamma], \tag{3.3}$$

The representative crack QQ' is also subjected to far-

field stresses σ_1 and σ_2. The stress intensity factor at the crack tips, Q and Q', is given by

$$K_I = \frac{F\sin\theta}{\sqrt{\pi(l+l^*)}} + \frac{\sqrt{\pi l}}{2}[\sigma_1+\sigma_2-(\sigma_1-\sigma_2)\cos 2(\theta-\gamma)] \quad (3.4)$$

where θ is the angle between the pre-existing defect and the tension crack, and $l^* = 0.27c$ (see Nemat-Nasser & Horii [1982b]). It was shown that the prediction by this simple model is in accord with the results of the model shown in Figure 4.

3.2 Crack growth based on stress corrosion

As mentioned in Section 2, the time-dependent crack growth is understood as stress corrosion crack growth. When the stress intensity factor attains the fracture toughness of rock, the brittle crack growth occurs. The condition for crack growth is given by,

$$K_I = K_c \quad (3.5)$$

where K_c is the fracture toughness, which is the material constant. If the stress intensity factor is below the fracture toughness, the relationship between the stress intensity factor and the velocity of crack growth is considered to satisfy (2.1).

By substituting the given maximum and minimum principal stresses σ_1 and σ_2 to (3.3) and (3.4), the stress intensity factor is obtained. The crack length just after the loading can be calculated with the condition for crack growth, $K_I = K_c$. By integrating (2.1) with respect to time, the relationship between time and crack length is obtained.

It has been clarified from experiments that creep behavior in brittle rock under compression is the result of the propagation and growth of microcracking which increase the strain that, in this study, is called crack strain. The average crack strain $\bar{\varepsilon}_{ij}^{C}$ is given by

$$\bar{\varepsilon}_{ij}^{C} = \frac{N}{V}\int_{S^C}\frac{1}{2}([u_i]n_j+[u_j]n_i)\,dS \quad (3.6)$$

N/V is the crack density, S^C is the surface of the crack including both tensile crack and initial sliding slit, n_i is the unit normal vector of the crack surface, and $[u_i]$ is the displacement jump across the crack surface. Note that in the simplified model shown in Figure 5, the effect of sliding along the initial defect is replaced by the concentrated forces. However, for the evaluation of the crack strain, the displacement jump along the initial defect must be evaluated and introduced into (3.6). To estimate the displacement jump along the initial defect and the microcrack emanated at the tip of the defect in Figure 5, Muskhelishvili method is available. For the proposed simple model, the volumetric crack strain is obtained from (3.6).

3.3 Fracture criterion

It is possible to predict the crack length and crack strain as a function of the time. However, the failure criterion is necessary to predict the failure time. As already explained, the localization of microcracking leads to final failure. To predict the localization, further modelling with special attention to interaction effects between microcracks is required. In this study, to avoid such an extra effort, the following failure criterion is proposed.

One of the possible measures for failure is the volumetric crack strain. That is, it is assumed that localization and failure occur when the volumetric crack strain reaches a critical value. In fact, Krantz reports that the volumetric crack strain is almost constant at a constant confining pressure for various values of axial compression and accordingly with various failure times. Another candidate is critical crack length. It is assumed that localization and failure occur when a length of growing microcrack attains its critical length.

It is considered that the volumetric crack strain and the crack length have a one to one relationship and these two criteria have a correlation. Localization and failure result from interaction between microcracks and are considered to occur at a certain stage of microcracking.

In this study, the second criterion is adopted and the critical crack length is selected so as to fit the relationship between failure time and axial stress observed by Krantz [1980] for various confining pressures.

4 COMPARISON WITH EXPERIMENTAL RESULTS OF TRIAXIAL CREEP TEST

4.1 Experimental results

Krantz also carried out triaxial creep tests on Barre granite with various pressures and axial stresses. Several tests at 0.1 MPa, 53 MPa, 100 MPa and 198 MPa confining pressure at 87% of the corresponding to fracture strengths were stopped at, or shortly after, the onset of tertiary creep. The samples were unloaded and internal sections were cut out for examinations of number of cracks, crack length, crack width, and crack orientation. This was conducted in the same way explained in Section 2. If the confining pressure is larger at a constant axial compression, the failure time is longer. If, on the other hand, the axial compression is larger at a constant confining pressure, the failure time is shorter (see, Figure 6). Krantz reports that the volumetric crack strain just before failure is more or less constant, independent of the

applied axial stress and various values of failure time at any particular confining pressure. The higher confining pressure causes the larger volumetric strain (see, Figure 7).

4.2 Comparison of prediction

In this subsection, numerical results by the proposed model are reviewed compared with experimental results by Krantz. The algorithm explained in the previous section is employed for computations.

At first, by substituting the given maximum and minimum principal stresses σ_1 and σ_2 to (3.3) and (3.4), the stress intensity factor is obtained. With the criterion of crack growth $K_I = K_c$, it is possible to calculate the brittle crack length just after the loading. By integrating (2.1) with respect to time, the relationship between time and crack length is obtained at the given stress condition. The failure time is predicted from fracture criterion with the critical length of the crack determined for the considered confining pressure. The failure time is obtained from the relationship between time and crack length. Next, the volumetric crack strain is calculated from (3.8).

The input parameters for the analytical model (see, Figure 4 and Figure 5) are the angle θ between a pre-existing defect and the growing tensile crack, the angle γ between the collinear splitting force F and σ_1-direction, the cohesive stress τ_c, the coefficient of friction μ, the length of pre-existing defect $2c$, the fracture toughness K_c, the crack density N/V, and the elastic modulus E. In the present study, the following values are used; $\theta = \gamma = 45^\circ$, $\tau_c = 0$ MPa, $\mu = 0$ so that the numerical results would be on the safe side. $2c = 150$ μm, $E = 10000$ MPa, which are determined through parametric study to fit the experimental data. A low value is used for the Young's modulus so as to fit the observed volumetric crack strain. In the present model, the effect of sliding of the pre-existing defect is replaced with the splitting forces as shown in Figure 5. Therefore, there is a possibility that the displacement jump of microcrack is underestimated. The ignored interaction effect is another possibility for the underestimation of the displacement jump.

The maximum value of the stress intensity factor shown in (3.4) occurs at $\gamma = 45^\circ$ for $\mu = 0$. At room temperature, the fracture toughness $Kc = 1$ MPam$^{1/2}$ and the stress corrosion crack growth indices $R = 0.0001$ and $n = 30$ for granite, which are selected referring to the table of the critical stress intensity factor of materials (see, for example, Atkinson [1984]). The crack density $N/V = 0.32$ mm^{-3}, which is estimated from the SEM observation by Krantz.

Figure 6 displays the predicted failure time for different axial compressive stress σ_1 with a certain constant confining pressure σ_2; σ_2 = (a) 53 MPa, (b) 100 MPa and (c) 198 MPa together with the experimental results by Krantz for comparison. With higher axial stress for a certain constant confining pressure, the crack velocity is faster. In the case of the confining pressure 53 MPa, the experimental results by Krantz are fitted if 130 μm is chosen as the failure crack length. A similar argument is available for different values of confining pressures. It is shown that the failure time can be predicted by the proposed model. The theoretical failure crack length is shorter than the observed length by Krantz. The observed length may include that of the pre-existing defect which is excluded in the model.

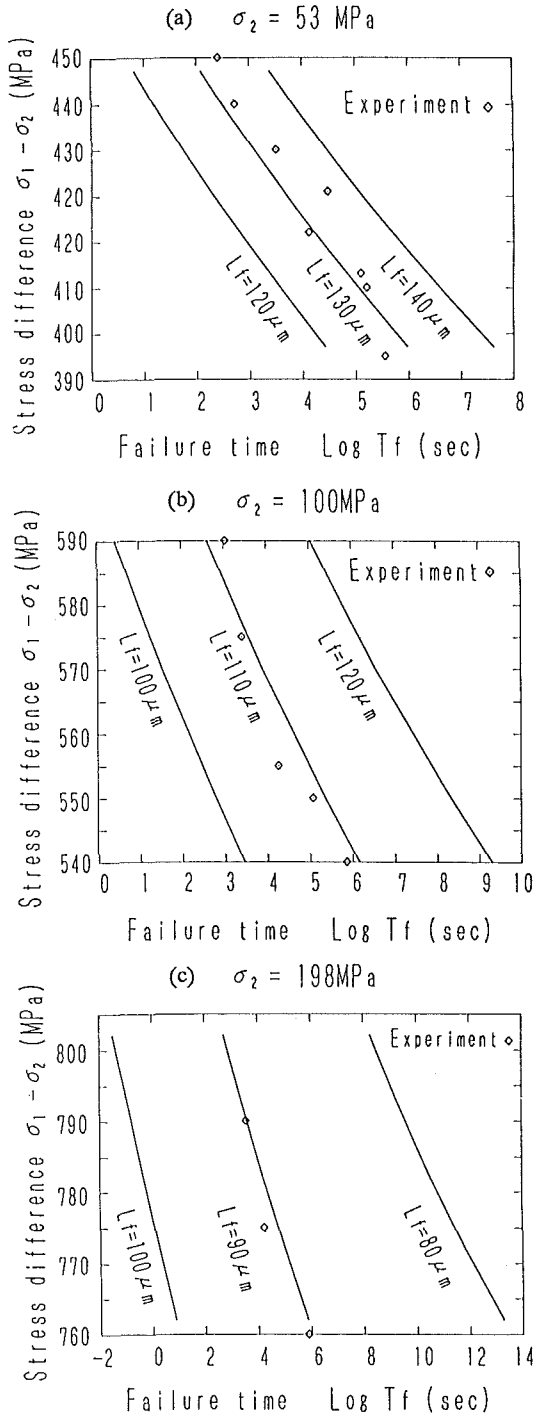

Figure 6 Stress difference vs. failure time

As mentioned in Subsection 3.3, the volumetric crack strain is roughly constant at a constant confining pressure with any axial compression and failure time. Figure 7 shows the prediction of volumetric crack strain just before failure for various confining pressures in which the experimental results by Krantz are also plotted. The numerical results coincide with those by Krantz.

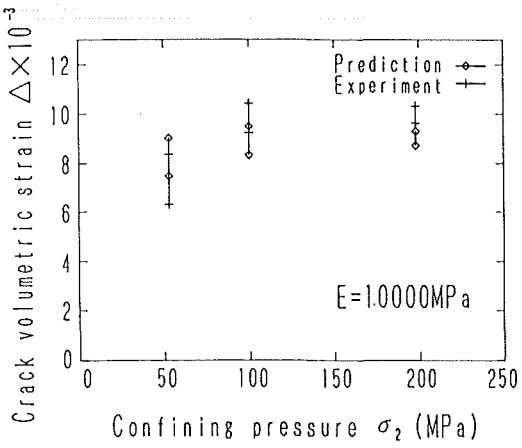

Figure 7 Confining pressure vs. volumetric strain

From the agreement between the numerical results and the experimental data, it is seen that the creep deformation and creep failure of hard rock are reproduced by the proposed simple model based on time-dependent growth of microcracks.

5 FINITE ELEMENT ANALYSIS FOR CREEP BEHAVIOR OF UNDERGROUND STRUCTURE

In the previous section, it is shown the numerical results by proposed model fitted the experimental data. In this section, a constitutive equation is derived on the basis of the model and implemented into a finite element program to analyze the creep behavior of rock structures at a great depth.

5.1 Constitutive equation

Consider an elastic solid of total volume V containing a set of cracks. The average stress and average strain in the solid are defined as

$$\bar{\sigma}_{ij} = \frac{1}{V}\int_V \sigma_{ij}\,dV, \qquad \bar{\varepsilon}_{ij} = \frac{1}{V}\int_V \varepsilon_{ij}\,dV, \tag{5.1}$$

The strain-displacement relation is given by

$$\varepsilon_{ij} = \frac{1}{2}(u_{i,j}+u_{j,i}) \tag{5.2}$$

where comma followed by an index denotes partial differentiation with respect to the corresponding coordinate. Since the material surrounding cracks is considered to be elastic and homogeneous,

$$\bar{\varepsilon}^M_{ij} = D^M_{ijkl}\bar{\sigma}_{kl} \tag{5.3}$$

where $D_{ijkl}{}^M$ and $\bar{\varepsilon}^M_{ij}$ are the elastic compliance and strain tensors for the elastic matrix. With the aid of the divergence theorem, it follows that,

$$\begin{aligned}\bar{\varepsilon}_{ij} &= D^M_{ijkl}\bar{\sigma}_{kl} \\ &\quad + \frac{1}{V}\int_{S^C}\frac{1}{2}([u_i]n_j+[u_j]n_i)\,dS \\ &= \bar{\varepsilon}^M_{ij}+\bar{\varepsilon}^C_{ij}\end{aligned} \tag{5.4}$$

where the second term in the right hand side of (5.4) is the average crack strain $\bar{\varepsilon}^C_{ij}$ explained in Section 3. This equation is rewritten as

$$\begin{aligned}\bar{\sigma}_{ij} &= C^M_{ijkl}\{\bar{\varepsilon}_{kl} - \bar{\varepsilon}^C_{kl}\} \\ &= C^M_{ijkl}\{\bar{\varepsilon}_{kl} \\ &\quad - \frac{1}{V}\int_{S^C}\frac{1}{2}([u_k]n_l+[u_l]n_k)\,dS\}\end{aligned} \tag{5.5}$$

where $C_{ijkl}{}^M$ is the elastic modulus tensor for the elastic matrix, which is given by

$$\begin{aligned}C^M_{ijkl} &= \frac{E\nu}{(1+\nu)(1-2\nu)}\delta_{ij}\delta_{kl} \\ &\quad + \frac{E}{2(1+\nu)}(\delta_{ik}\delta_{jl}+\delta_{il}\delta_{jk})\end{aligned} \tag{5.6}$$

where E and ν are the Young's modulus and Poisson's ratio respectively, and δ_{ij} is the Kronecker's delta.

The equation (5.5) is a general expression of the overall strain-stress tensor for a body with displacement discontinuities. To obtain the solution of coupled equations (5.3), (5.4), (5.5) and (5.6), incremental equations are employed. The incremental expressions is derived from (2.1) as

$$\Delta l = A(K_I)^n \Delta t \tag{5.7}$$

where Δt and Δl are the increments of time and length. At a certain time t with known distribution of stress and crack length, the stress intensity factor is obtained from the proposed model and the increment of crack length is calculated from (5.7). With updated crack length, a new constitutive equation is obtained from (5.4). The Euler's method is employed to obtain the relationship between time and crack length. The increment of crack length calculated at each time step is summed up with sufficiently small time increment.

The algorithm of finite element analysis to predict the crack length is shown as follows.

(1) The elastic stresses and strains are obtained by the elastic analysis at each element with finite element method (FEM) for the given stress condition.

(2) The maximum and minimum principal compressions and the angle of maximum principal stress are derived from the stresses obtained above.

(3) By substituting the maximum and minimum principal compressions to (3.3) and (3.4), the stress intensity factor is calculated for a certain crack length.

(4) On the basis of the condition for the crack growth $K_I = K_c$ shown in Subsection 3.2, the initial crack length just after loading is obtained at each element.

(5) For a given increment of time, the increment of crack length is calculated with (5.7). Then the crack length at $t+\Delta t$ is obtained by adding the incremental length to the previous length.

(6) The crack strain is calculated by substituting the displacement jump across the crack surface to (3.6).

(7) By substituting the average and crack strain to the general constitutive equation (5.5), new stress distribution is obtained.

The process from (5) to (7) is repeated to obtain solutions with increasing time.

5.2 Results of finite element analysis

To check whether the proposed constitutive model can reproduce the long time behavior of rock structures, crack length under the given loading condition is calculated as a function of time at different temperatures by the finite element analysis explained in the previous subsection. A problem of elliptical excavation at 2000 m depth is analyzed at different temperatures; room temperature, 100 °C and 400 °C. The considered region for numerical analysis and the boundary condition at 2000 m depth are shown in Figure 8. Noted that the gravitational force is ignored in the considered region. Earth pressure is applied as a boundary condition. The material of rock is assumed to be granite. Taking the symmetry into account, it is enough to solve a quarter of the considered region.

As mentioned in Subsection 2.2, the velocity of crack growth is greatly affected by temperature and environmental conditions such as humidity and pH. Figure 2 shows that as the temperature increases, the line illustrating the relationship between the stress intensity factor and the velocity of crack growth shifts from right to left, while there is little change of the slope of this line. This implies that only A is dependent on temperature among the material constants n and A in (2.1). In the present study, A is set to be 10^{-4}, 1.0 and 10^{8} for room temperature, 100 °C and 400 °C respectively with reference to the laboratory experiments by Atkinson [1984]. The pre-existing defects are assumed to be 45° to the axis of maximum principal stress at each element, since maximum value of the stress intensity factor occurs at this angle for $\mu = 0$. Other input data are the same as those given in Subsection 4.2.

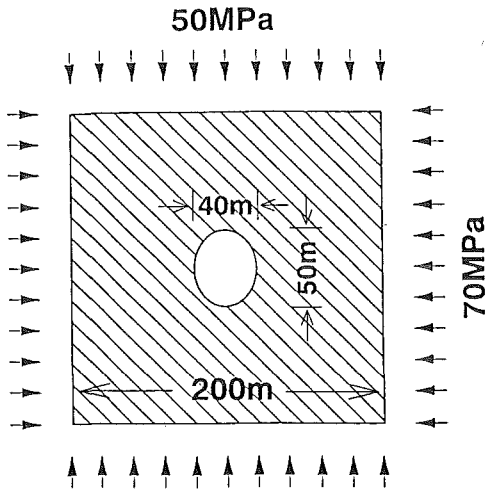

Figure 8 Elliptical excavation at 2000 m depth

The crack length in rock is calculated by the process shown in the previous subsection. Figure 9 shows the length and orientation of cracks just after loading, after one day, after 100 days and after 3000 years at 400 °C. It is seen that, crack length increases with increasing time. The crack length around top of the excavations where the stress concentration occurs is higher than those of other parts. In Figure 9, the longest crack exists at the top of excavation and its length, for example, is about 100 μm just after loading (see Table 1).

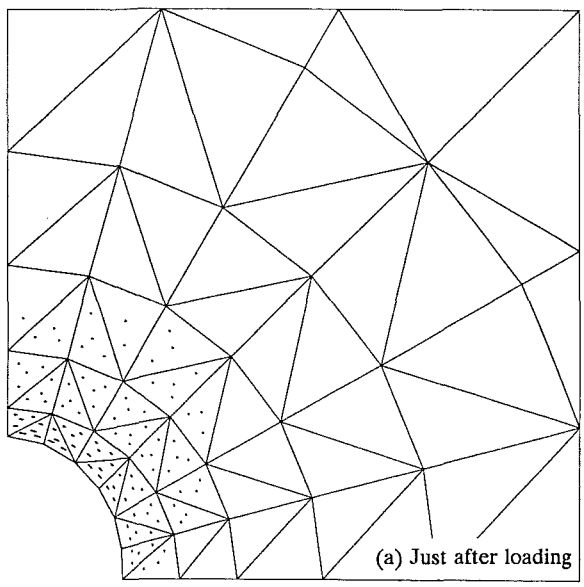

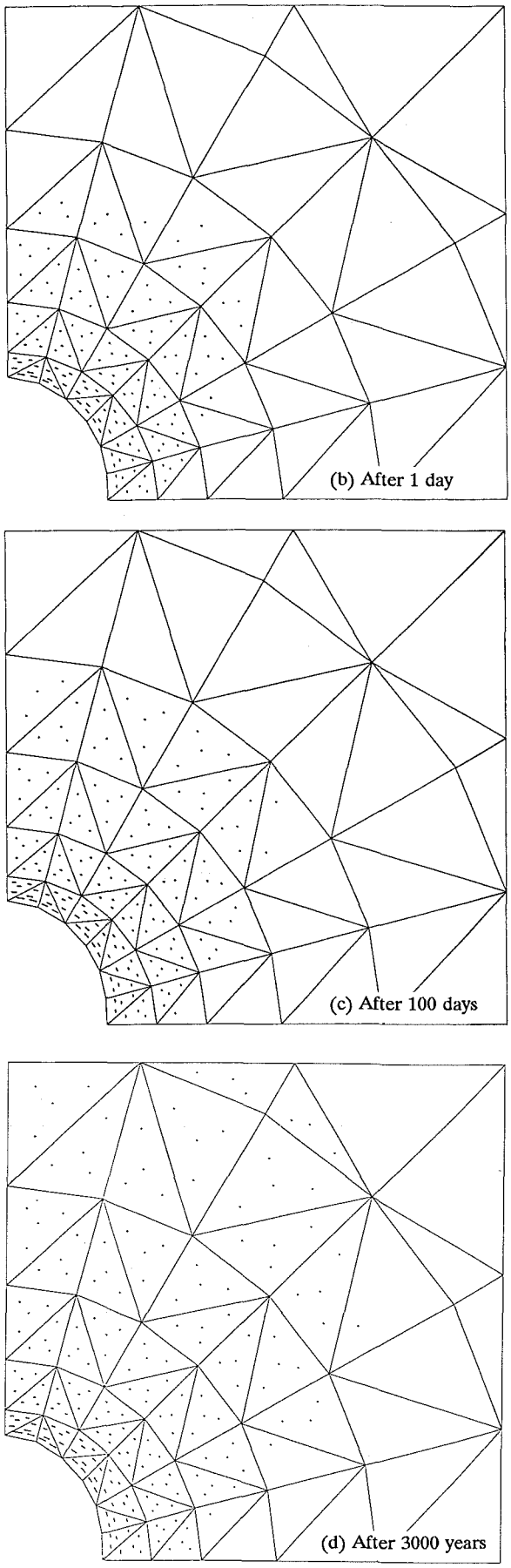

Figure 9 Length and orientation of cracks

Table 1 shows the crack length at the top of excavation at room temperature, 100 °C and 400 °C just after loading, after one day, after 100 days, after 30 years and after 3000 years. It shows that if the temperature is higher, the crack growth is faster. If the creep failure of rock occurs when the crack length reaches 100 μm, rock at room temperature does not fail even after 3000 years. However, in the case that the temperature is 100 °C, rock would fail between after 100 days and 30 years. In the case of 400 °C, it fails just after loading.

Table 1 Crack length at the top of excavation

Time / Temperature	1 second	1 day	100 days	30 years	3000 years
t=20°C	25.62 μm	56.44 μm	68.80 μm	81.36 μm	93.72 μm
t=100°C	50.60 μm	81.36 μm	93.72 μm	105.58 μm	116.82 μm
t=400°C	99.72 μm	127.34 μm	137.04 μm	145.96 μm	154.08 μm

Figure 10 shows the relationship between time and stress intensity factor at the top of the excavation for various temperatures. The stress intensity factor decreases with increasing time in all cases. When temperature is high, the crack propagates and grows at an early stage. According to the equation (3.4), the longer crack causes the stress intensity factor to decrease under compression. Therefore the stress intensity factor at a higher temperature is smaller.

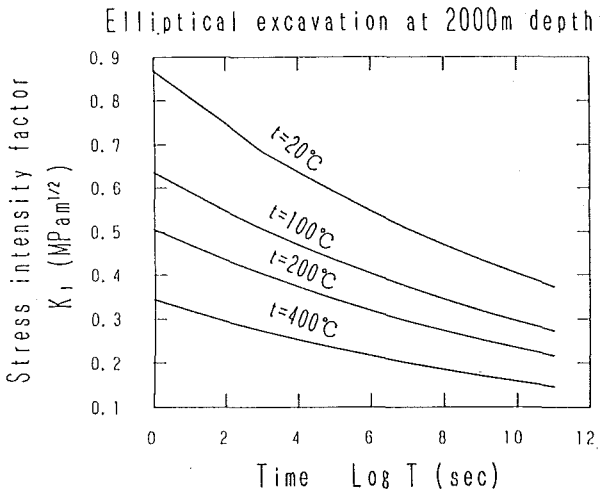

Figure 10 Stress intensity factor vs. time

6 SUMMARY AND CONCLUSION

In this study, an analytical model is proposed to predict the creep deformation and creep failure of rock under compression. The model is based on the fact that the creep phenomena are governed by the growth of microcracks which emanates from the pre-existing defects in rock. The proposed model is simple

and has few parameters to predict the creep behavior. They are determined from the data given by Krantz [1979, 1980] and Atkinson [1984].

First, with the proposed model, the reproduction of the laboratory experiment for granite by Krantz is carried out. The relationship between time and crack length and the volumetric crack strain are calculated at a constant confining pressure for various axial compressions. The numerical results are compared with the empirical data by Krantz. By taking a certain length as the failure length, it is possible to reproduce the experimental data.

Next, the constitutive equation for creep phenomena of rock is derived from the proposed micromechanical model and is implemented into a finite element analysis program to analyze creep behavior. The problem of elliptical excavation under hydrothermal conditions is analyzed and the long-term crack length field is predicted at different times and temperatures. At the same time, the stress intensity factor as a function of time is shown at different times after loading.

The results of the finite element analysis indicate a possibility that rock may fail due to the effect of high temperature. Since, as shown in Subsection 4.2, the crack velocity of rock under hydrothermal environment is fast, this is considered to affect the underground structures.

The finite element program for creep behavior developed in the present study enables us to analyze the stability of any underground structures in rock.

REFERENCES

1. Atkinson,B.K. (1984) Subcritical crack growth in geological materials, J. Geophys. Res. vol.89, no.B6, pp.4077-4114

2. Horii,H. & Nemat-Nasser,S. (1985) Compression-Induced microcrack growth in brittle solids: axial splitting and shear failure, J. Geophys. Res. vol.90, no.B4, pp.3105-3125

3. Horii,H. & Nemat-Nasser,S. (1986) Brittle failure in Compression: Splitting, Faulting and Brittle-Ductile Transition, Phil. Trans. Roy. Soc. London. vol.319, pp.337-374

4. Krantz,R.L. (1979) Crack growth and development during creep of Barre granite, J. Rock Mech. Min.Sci & Geomech. Abstr. vol.16, pp.23-35

5. Krantz,R.L. (1980) The effects of confining pressure and stress difference on static fatigue of granite, J. Geophys. Res, vol.85, no.B4, pp.1854-1866

6. Nemat-Nasser,S. & Horii,H. (1982a) Compression-induced nonplanar crack extension with application to splitting, exfoliation, and rock burst, J. Geophys. Res, vol.87, no.B8, pp.6805-6821

7. Nemat-Nasser,S. & Horii,H. (1982b) Overall moduli of solids with microcracks: load-induced anisotropy, J. Mech. Phys. Solids, vol.31, no.2, pp.155-171

8. Tapponnier, P. & W. F. Brace. (1976) Development of stress-induced microcracks in Westerly granite, Int. J. Rock Mech. Min. Sci. Geomech. Abstr, vol.13, pp.61-85